Materials Research Letters

ISSN: (Print) 2166-3831 (Online) Journal homepage: https://www.tandfonline.com/loi/tmrl20

Anisotropic exchange in Nd–Fe–B permanent magnets

Qihua Gong, Min Yi, Richard F. L. Evans, Oliver Gutfleisch & Bai-Xiang Xu

To cite this article: Qihua Gong, Min Yi, Richard F. L. Evans, Oliver Gutfleisch & Bai-Xiang Xu (2020) Anisotropic exchange in Nd–Fe–B permanent magnets, Materials Research Letters, 8:3, 89-96, DOI: 10.1080/21663831.2019.1702116

To link to this article: https://doi.org/10.1080/21663831.2019.1702116

MATER. RES. LETT.
2020, VOL. 8, NO. 3, 89–96
https://doi.org/10.1080/21663831.2019.1702116

MATERIALS RESEARCH LETTERS
Taylor & Francis
Taylor & Francis Group

ORIGINAL REPORT

Anisotropic exchange in Nd–Fe–B permanent magnets

Qihua Gong[a], Min Yi [a,b], Richard F. L. Evans[c], Oliver Gutfleisch [a] and Bai-Xiang Xu[a]

[a]Institute of Materials Science, Technische Universität Darmstadt, Darmstadt, Germany; [b]State Key Lab of Mechanics and Control of Mechanical Structures & Key Lab for Intelligent Nano Materials and Devices of Ministry of Education & College of Aerospace Engineering, Nanjing University of Aeronautics and Astronautics (NUAA), Nanjing, People's Republic of China; [c]Department of Physics, The University of York, York, UK

ABSTRACT

The exchange is critical for designing high-performance Nd–Fe–B permanent magnets. Here we demonstrate through multiscale simulations that the exchange in Nd–Fe–B magnets, including bulk exchange stiffness (A_e) in $Nd_2Fe_{14}B$ phase and interface exchange coupling strength (J_{int}) between $Nd_2Fe_{14}B$ and grain boundary (GB), is strongly anisotropic. A_e is larger along crystallographic *a*/*b* axis than along *c* axis. Even when the GB Fe_xNd_{1-x} has the same composition, J_{int} for (100) interface is much higher than that for (001) interface. The discovered anisotropic exchange is shown to have profound influence on the coercivity. These findings enable more freedom in designing Nd–Fe–B magnets by tuning exchange.

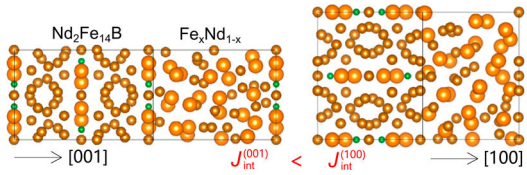

ARTICLE HISTORY
Received 10 August 2019

KEYWORDS
Permanent magnets; grain boundary; interface exchange; coercivity; multiscale simulations

IMPACT STATEMENT

Bulk exchange stiffness in $Nd_2Fe_{14}B$ and interface exchange coupling strength between $Nd_2Fe_{14}B$ and grain boundary are found strongly anisotropic, which have profound influence on the coercivity of Nd–Fe–B magnets.

1. Introduction

High-coercivity permanent magnets are indisputably one of the critical materials indispensible for modern technologies in which electrical energy is converted to motion with a high efficiency or *vice versa* [1–4]. Among all the available permanent magnets, nowadays Nd–Fe–B (neodymium–iron–boron) is the most powerful and commercially important magnet. However, for certain applications such as hybrid/electric vehicles where the increased operating temperatures of 120–160°C are common, the coercivity of sintered Nd–Fe–B magnets ($\sim$1.2 T) is too low. Improving the coercivity of Nd–Fe–B magnets without the usage of heavy rare earth elements (e.g. Dy, Tb) and without sacrificing remanence is still of great importance [5–7].

Coercivity is an extrinsic property. In Nd–Fe–B magnets, it is determined by the interplay of intrinsic magnetic properties of $Nd_2Fe_{14}B$ phase (the saturation magnetization M_s, magnetocrystalline anisotropy constant K_1, and the exchange stiffness A_e) and the microstructure including grain boundary (GB) and intergranular phases [5–9]. Microstructure engineering has been explored to design high-coercivity Nd–Fe–B magnets, e.g. optimizing the grain shape and reducing the grain size to decrease the local effective demagnetization factor N_{eff} [10–14], doping $Nd_2Fe_{14}B$ grain or its surface with Dy or Tb to increase the anisotropy field H_A [15–18], deceasing M_s of GB to make $Nd_2Fe_{14}B$ grains exchange decoupled by GB diffusion [19–21], etc.

Based on the micromagnetic theory, the coercivity of Nd–Fe–B magnets can be tailored by controlling the distribution of three parameters, i.e. M_s, K_1, and A_e whose spatial variation represents the magnetic microstructure. In contrast to the efforts on tuning N_{eff}, H_A, and GB M_s,

CONTACT Min Yi yi@mfm.tu-darmstadt.de Institute of Materials Science, Technische Universität Darmstadt, 64287 Darmstadt, Germany .

Supplemental data for this article can be accessed here. https://doi.org/10.1080/21663831.2019.1702116

the critical role of exchange (A_e) is not fully explored or less focused for sintered and hot-pressed magnets, in contrast to the situation of exchange-spring magnets [22–24]. The associated challenge is mainly attributed to the difficulty of measuring exchange experimentally, including bulk exchange stiffness and interface exchange coupling strength, in Nd–Fe–B magnets. The experimental determination of M_s and K_1 is much easier [25–28]. Even though the decrease of GB M_s to improve coercivity is qualitatively explained by the exchange decoupling [19–21], the underlying quantitative interface exchange behavior still remains to be explored.

A_e in $Nd_2Fe_{14}B$ phase is estimated as 7.7 pJ/m by using K_1 and the domain wall energy which is calculated from the measured M_s and domain width through the Bodenberger–Hubert formula [26]. This value is widely adopted and never questioned. As for the interface exchange, both first-principles calculations and experiments suggest that the exchange coupling is positive in $Nd_2Fe_{14}B(001)/\alpha$-Fe interface, while negative in $Nd_2Fe_{14}B(100)/\alpha$-Fe interface [29–32]. But the favorable and extremely thin (several nanometers) GB phase in sintered and hot-pressed Nd–Fe–B magnets is often amorphous, resulting in the local atomic arrangements different from α-Fe and thus possibly distinct interface exchange behavior. In addition, electron microscopic analysis has confirmed that GB composition is anisotropic, i.e. GB phase parallel to the *c*-plane contains lower concentration of Fe than that perpendicular to the *c*-plane [33–35]. Whether and how the $Nd_2Fe_{14}B$/GB interface orientation and GB composition anisotropy will influence the interface exchange is yet unknown quantitatively.

In this work, through first-principles calculations and atomistic spin model (ASM) simulations, we provide the hitherto missing information on the quantitative exchange anisotropy in Nd–Fe–B permanent magnets. Specifically, we demonstrate the strong anisotropy in the exchange stiffness of $Nd_2Fe_{14}B$ phase and the interface exchange coupling strength between $Nd_2Fe_{14}B$ and GB. We discover the 'double anisotropy' phenomenon related to GB, i.e. in addition to the experimentally confirmed GB magnetization anisotropy, the $Nd_2Fe_{14}B$/GB interface exchange coupling is also anisotropic. In detail, we perform ASM simulations of $Nd_2Fe_{14}B$ to calculate the temperature-dependent exchange stiffness along different crystallographic axes. Moreover, we carry out first-principles calculations to relax the $Nd_2Fe_{14}B$/GB interface structure and unravel the interface orientation-dependent exchange coupling strength. The influence of exchange anisotropy on coercivity is revealed by micromagnetic simulations. More generally, these discoveries may enable more freedom in the design of Nd–Fe–B magnets by tuning exchange.

2. Methodology

The temperature-dependent A_e of $Nd_2Fe_{14}B$ is evaluated through ASM simulation by using VAMPIRE [36] based on the atomistic spin Hamiltonian which is proposed and parameterized previously [37–41]. Detailed formulations for the ASM of $Nd_2Fe_{14}B$ are provided in the Supplemental Material. The spin dynamics approach and the Heun integration scheme in VAMPIRE [36] are utilized to calculate the domain-wall width. A sharp Bloch-like domain wall (wall plane perpendicular to *x* axis) and Néel-like domain wall (wall plane perpendicular to *z* axis) in the middle of the sample with $N_x \times N_y \times N_z = 40 \times 5 \times 5$ and $N_x \times N_y \times N_z = 5 \times 5 \times 40$ unit cells is set as the initial condition, respectively. With the demagnetizing field included in the ASM simulations, the system is relaxed from this initial condition by 100,000 steps (time step: 1 fs). The final domain configuration is obtained by averaging the magnetic moment distribution of 100 states at 90.1, 90.2, 90.3, . . . , 100 ps.

First-principles calculations are carried out by using VASP (Vienna *Ab-initio* Simulation Package). According to previous studies [30,32,37,42–44], an open-core pseudopotential for Nd is used, with the 4*f* electrons put in the core and not treated as valence electrons. The cutoff energy is set as 500 eV. Based on the energy convergence test, a $3 \times 3 \times 1$ and $1 \times 3 \times 2$ *k*-point mesh is used for $Nd_2Fe_{14}B(001)/Fe_xNd_{1-x}$ and $Nd_2Fe_{14}B(100)/Fe_xNd_{1-x}$, respectively. For the relaxation of $Nd_2Fe_{14}B/Fe_xNd_{1-x}$, the convergence criteria for the maximum force on each atom and the total energy are 0.03 eV/Å, and 0.05 meV, respectively. In the self-consistent calculations of the total energy, an energy convergence criteria of 0.01 meV is used.

Micromagnetic simulations are performed by using MuMax [45]. There are four kinds of energy considered in micromagnetics, which are exchange energy, anisotropy energy, Zeeman energy, demagnetization energy. The cell size is set as 1 nm, which is smaller than the exchange length and thus reasonable. The reversed curves are calculated by using the conjugate gradient method to find the energy minimum. The external field (H_{ex}) along *z* axis is applied as a stepwise field with a step of 0.01 T.

3. Results and discussion

Since the exchange stiffness is highly related to the domain wall, we first calculate the domain wall profile. The ASM simulated Bloch- and Néel-like configurations at different temperatures are shown in Figure 1(a,b), respectively. Different from the previous work [38,39], domain walls with the tilting angle θ_0 at low temperatures

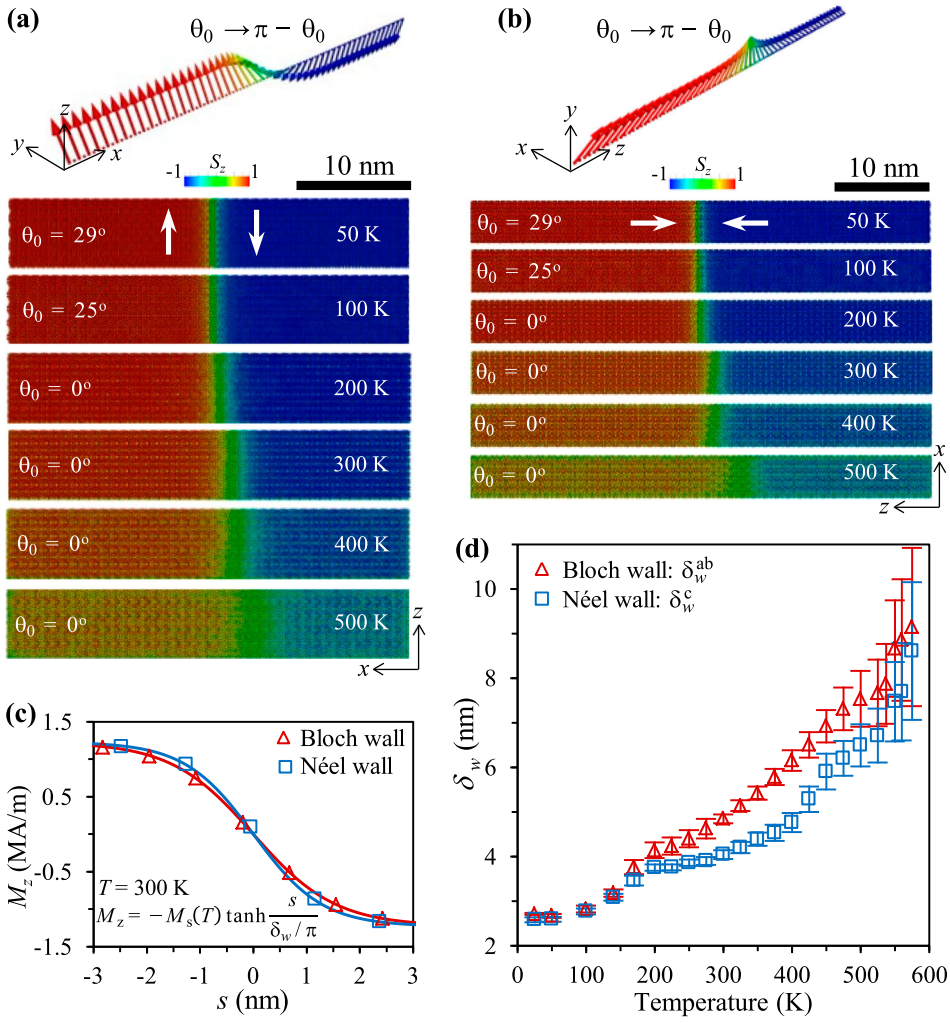

Figure 1. ASM simulated temperature-dependent domain wall configurations displayed by the distribution of atomistic magnetic moments (easy axis tilted from *z*-axis with a angle θ_0): (a) Bloch-like wall and (b) Néel-like wall. (c) The distribution of macroscopic magnetization component (M_z) along *x* axis in (a) and *z* axis in (b). (d) Domain wall width δ_w at different temperatures.

is also calculated. It is obvious that both walls become wider when the temperature increases. After mapping the atomistic magnetic moments in Figure 1(a,b) to the continuum magnetization, we fit the domain wall by a hyperbolic function [46], as shown in Figure 1(c) and Figures S1 and S2 (Supplementary Material). In this way, the temperature-dependent domain wall width δ_w is determined and summarized in Figure 1(d). It should be noted that at 300 K, the exchange stiffness A_e [26,46,47] and K_1 [26,46] in the literature corresponds to an estimated $\delta_w = \pi\sqrt{A_e/K_1}$ as 3.63–5.31 nm. Our calculated δ_w at 300 K falls well in this range. It can be seen from Figure 1(d) that after the spin reorientation temperature around 150 K, both the Bloch wall width (δ_w^{ab}) and Néel wall width (δ_w^{c}) increase with temperature. However, δ_w^{ab} is larger than δ_w^{c}, indicating the anisotropic nature of domain wall width in $Nd_2Fe_{14}B$.

According to the continuum micromagnetic theory [46], the domain wall profile is generally governed by

$$x(\theta, T) = \sqrt{A_e^{ab}(T)} \int_{\theta_0}^{\theta} [F(\Theta, T) - F(\theta_0, T)]^{-(1/2)}\, d\Theta, \tag{1}$$

and

$$z(\theta, T) = \sqrt{A_e^{c}(T)} \int_{\theta_0}^{\theta} [F(\Theta, T) - F(\theta_0, T) + 0.5\mu_0 M_s^2(T)(\cos\Theta - 1)\cos\Theta]^{-(1/2)} d\Theta, \tag{2}$$

for Bloch walls and Néel walls, respectively. $F(\Theta, T)$ is the temperature-dependent magnetocrystalline anisotropy energy as a function of the polar angle Θ. $M_s(T)$ is the temperature-dependent saturation magnetization. Both

$F(\Theta, T)$ and $M_s(T)$ have been determined previously [37,40]. In Equation (2), the additional term regarding to M_s is originated from the demagnetization energy in the Néel wall. In most cases, there is no analytic solution for Equations (1) and 2. Since x and z are monotonic functions of θ in Equations (1) and (2), there exists an inverse function $\theta(x, T)$. Therefore, after numerical integration of Equations (1) and (2) with various $A_e^{ab}(T)$ or $A_e^c(T)$, we attain a series of theoretical curves with s (s: x or z) as a function of $M_z = M_s(T)\cos(\theta(x, T))$. Then we optimize $A_e^{ab}(T)$ and $A_e^c(T)$ through the least-square method by comparing the simulation data to the theoretical curves. In Figure S3 (Supplementary Material), we plot both the simulation data points and the theoretical curves (solid lines) with the optimum $A_e^{ab}(T)$ and $A_e^c(T)$.

The calculated exchange stiffness is summarized in Figure 2(a). It is obvious that $A_e^{ab}(T)$ is higher than $A_e^c(T)$, indicating the anisotropic exchange stiffness in $Nd_2Fe_{14}B$ and agreeing with the previous report [39]. This anisotropic A_e is intrinsically attributed to the tetragonal crystal structure of $Nd_2Fe_{14}B$. At 300 K, $A_e^{ab}(T)$ and $A_e^c(T)$ are estimated as 10.2 and 7.7 pJ/m, respectively. These values are in accordance with those used in micromagnetic simulations and experimentally determined ones [26,46]. A_e is found to decrease much faster at higher temperatures. The scaling behavior of $A_e(T)$ with respect to the normalized magnetization m is presented in Figure 2(b). It is found that fitting the data gives a scaling law $A_e(T) \propto m^{1.2}$.

Another important exchange-related phenomenon, we have to explore is the interface exchange coupling strength (J_{int}) between GB phase and $Nd_2Fe_{14}B$, which is thought to play a critical role in the determination of coercivity of Nd–Fe–B magnets. Here, first-principles calculations are performed to estimate J_{int}. Following the experimental observation [34,35,48–50], we take Fe_xNd_{1-x} with different Fe content as the model GB. The $Nd_2Fe_{14}B$/GB interface is set as (001) and (100) surface of $Nd_2Fe_{14}B$, as shown in Figure 3(a,b), respectively. Nd atoms in Fe_xNd_{1-x} are initially randomly distributed in a bcc Fe structure. Five different random distributions are calculated and the associated results are averaged. The system lattice parameters in the plane parallel to the interface, as well as the atom position and lattice parameters of $Nd_2Fe_{14}B$, is fixed. The structure of GB Fe_xNd_{1-x} is relaxed by two steps. Firstly, only the distance between $Nd_2Fe_{14}B$ and Fe_xNd_{1-x} is relaxed (d in Figure 3(a)). Then both the atomic position and the lattice parameter along the axis perpendicular to the interface are fully relaxed. The typical relaxed structure is shown in Figure 3(a,b). It can be seen that after relaxation, Fe_xNd_{1-x} becomes amorphous-like, in accordance with

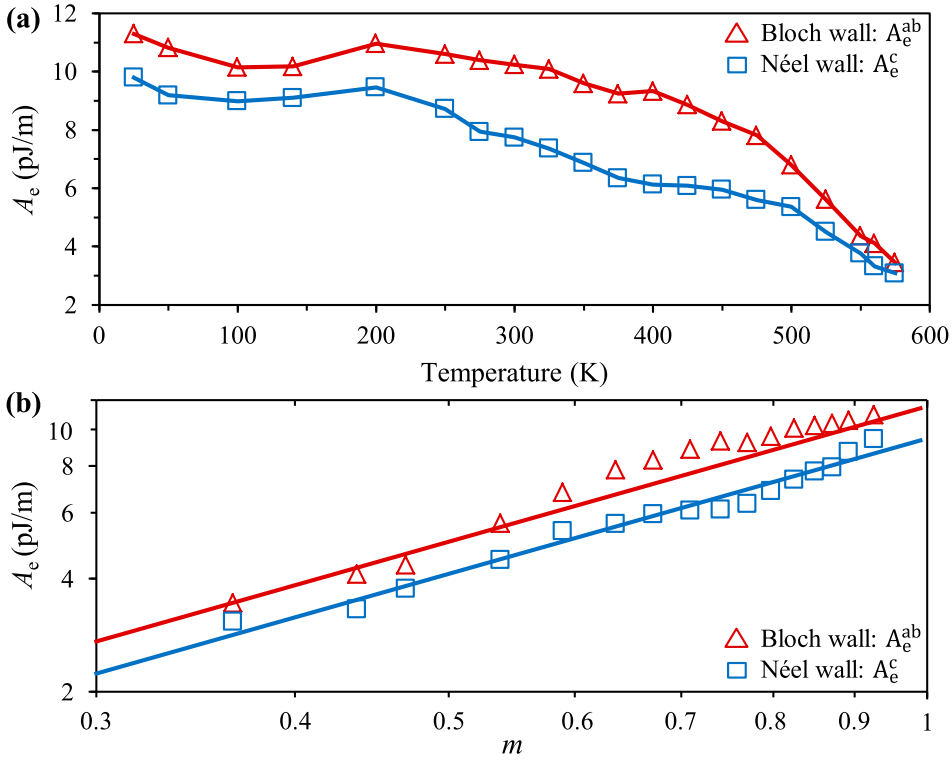

Figure 2. Exchange stiffness (A_e) of $Nd_2Fe_{14}B$ calculated by ASM simulation: A_e as a function of (a) temperature T and (b) normalized magnetization $m = M_s(T)/M_s(T = 0)$. The fitting lines in (b) $\propto m^{1.2}$.

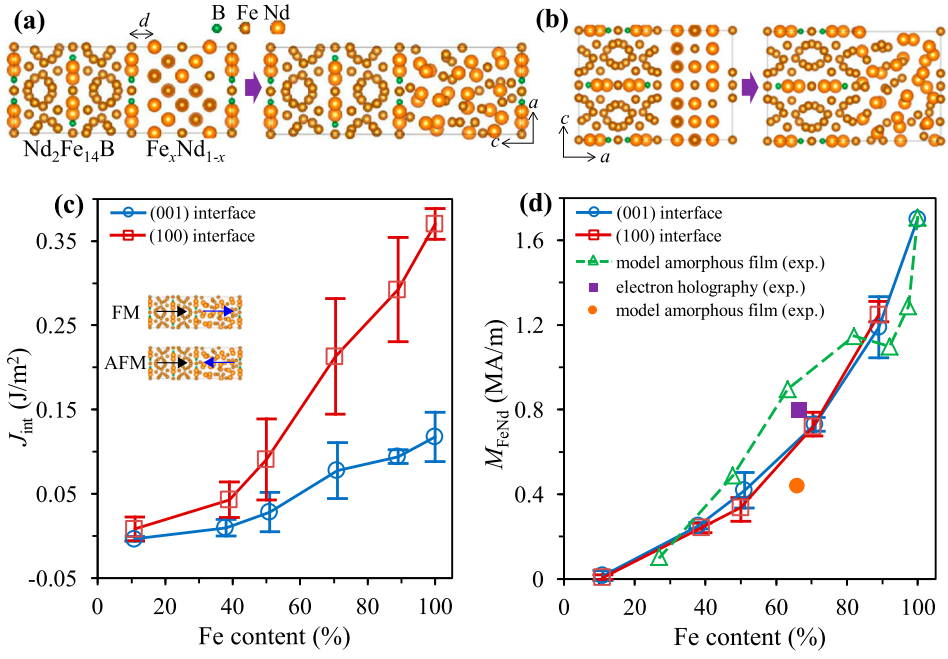

Figure 3. Interface exchange coupling strength (J_{int}) in $Nd_2Fe_{14}B$/GB evaluated by first-principles calculation. Unrelaxed and relaxed structure of $Nd_2Fe_{14}B/Fe_xNd_{1-x}$ system with interface located at (a) (001) plane and (b) (100) plane. (c) J_{int} and (d) magnetization of Fe_xNd_{1-x} (M_{FeNd}) as a function of Fe content x for both (001) and (100) interfaces. The experimental data in (d) are taken from the literature [48–50].

the experimental observation of thin amorphous GB in Nd–Fe–B magnets [33].

After obtaining the relaxed structure, we estimate J_{int} between $Nd_2Fe_{14}B$ and GB Fe_xNd_{1-x} by comparing the energy difference between the ferromagnetic (E^{FM}) and antiferromagnetic (E^{AFM}) configurations as illustrated in the inset of Figure 3(c), i.e. $J_{int} = (E^{AFM} - E^{FM})/2S$ with S as the interface area. The calculated J_{int} for both (001) and (100) interfaces is summarized in Figure 3(c). It is found that J_{int} is positive for both interfaces, indicating ferromagnetic coupling between GB Fe_xNd_{1-x} and $Nd_2Fe_{14}B$. It should be noted that in the case of (100) interface, if the GB phase is kept as α-Fe or not fully relaxed to be amorphous-like [29–32], J_{int} is negative and the antiferromagnetic coupling dominates. In contrast, our results here reveal that if GB is amorphous-like (i.e. the experimental case when GB is as thin as several nanometers), ferromagnetic coupling between $Nd_2Fe_{14}B$ and GB still remains for the (100) interface. Most importantly, even when the Fe content is the same, J_{int} is much higher for (100) interface than for (001) interface, indicating strong anisotropy in the interface exchange coupling.

Previous experiments have confirmed that the Nd-containing GB in the (100) surface of $Nd_2Fe_{14}B$ grain contains much higher Fe (i.e. higher magnetization) than those in the (001) surface [33–35]. Therefore, if the anisotropy in GB magnetization is considered, J_{int} will be even more anisotropic due to the increasing J_{int} with Fe content. This GB/$Nd_2Fe_{14}B$ interface orientation induced 'double anisotropy' (i.e. anisotropy in both magnetization and J_{int}) is expected to have a remarkable influence on the coercivity of Nd–Fe–B magnets. The magnetization of Fe_xNd_{1-x} GB phase (M_{FeNd}) as a function of Fe content is also calculated and shown in Figure 3(d). The calculated M_{FeNd} agrees well with the experimental reports [48–50]. It can be also seen that regardless of the interface orientation, M_{FeNd} only depends on the Fe content.

In order to evaluate the influence of the above anisotropy (i.e. exchange anisotropy in A_e and J_{int}, and GB composition anisotropy) on the coercivity ($\mu_0 H_c$) of Nd–Fe–B magnets, we further carry out micromagnetic simulations of model microstructures by using MuMax [45], as shown in Figure 4. For the exchange anisotropy, the effective field due to the bulk exchange within the $Nd_2Fe_{14}B$ grain is reformulated (using a 6-neighbor small-angle approximation) as

$$\mathbf{B}^{B}_{exch} = 2\frac{A_e^{ab}}{M_s}\sum_{i\in a \text{ or } b}\boldsymbol{\mathcal{M}}_i + 2\frac{A_e^{c}}{M_s}\sum_{i\in c}\boldsymbol{\mathcal{M}}_i, \quad (3)$$

in which $\boldsymbol{\mathcal{M}}_i = (\mathbf{m}_i - \mathbf{m})/\Delta_i^2$ with Δ_i as the mesh size along i direction, $\mathbf{m}$ as the magnetization unit vector of the current cell, and $\mathbf{m}_i$ as the magnetization unit vector of the neighbor cell along i direction. Similarly, the

effective field (due to the exchange interaction between $Nd_2Fe_{14}B$ and GB) which is exerted on $Nd_2Fe_{14}B$ can be reformulated as

$$\mathbf{B}_{\text{exch}}^{\text{Int}} = 2\frac{A_{\text{int}}^{ab}}{M_s}\sum_{i\in a \text{ or } b}^{\mathbf{m}_i\text{inGB}} \boldsymbol{\mathcal{M}}_i \quad \text{and} \quad 2\frac{A_{\text{int}}^{c}}{M_s}\sum_{i\in c}^{\mathbf{m}_i\text{inGB}} \boldsymbol{\mathcal{M}}_i \quad (4)$$

for the (100) and (001) interface, respectively. A_{int} is the inter-region exchange parameter as defined in MuMax [45], which is an indicator of J_{int} in Figure 3(c). The bulk exchange of GB phase is isotropic and estimated as $A_e^{\text{GB}} \sim \epsilon(\mu_0 M_{\text{GB}})^2$ with $\epsilon = 5.41\,\text{pJm}^{-1}\text{T}^{-2}$ [34].

The effect of anisotropic A_e in $Nd_2Fe_{14}B$ is explored in a single grain model with GB at different surfaces, as shown in Figure 4(a,b). It can be seen that for GB on the (100) interface, the anisotropic exchange $A_e^{ab} = 10.2$ pJ/m and $A_e^{c} = 7.7$ pJ/m results in much higher coercivity than the isotropic case $A_e = 7.7$ pJ/m. In contrast, for GB on the (001) surface, the anisotropic exchange leads to much lower coercivity than the isotropic case $A_e = 10.2$ pJ/m. These results indicate that the anisotropic exchange stiffness of $Nd_2Fe_{14}B$ has obvious influence on the coercivity, and the influence also depends on the $Nd_2Fe_{14}B$/GB interface orientation.

The determination of A_{int} in micromagnetics is non-trivial. In most literature on micromagnetic simulations of exchange-coupled behavior, A_{int} is chosen as the same as the bulk value, or is artificially tuned to study its influence. Skomski presented a continuum method to estimate the effective exchange between grains [24]. However, in the case of interface, the methodology for transferring first-principles results (J_{int}) to the continuum micromagnetic interface parameters (A_{int}) is unattainable at present. Here, A_{int} is assumed to be proportional to J_{int}, and its value along a or b axis is set as $A_{\text{int}}^{ab} = 5\,\text{pJ/m}$ for ab-GB with 80% Fe ($M_{\text{GB}}^{ab} = 1\,\text{MA/m}$). The c-GB contains less Fe, i.e. 60% Fe ($M_{\text{GB}}^{c} = 0.55\,\text{MA/m}$). According to J_{int} in Figure 3(c), A_{int}^{c} is estimated as one fifth of A_{int}^{ab}, i.e. 1 pJ/m. The influence of anisotropy in exchange (A_e and J_{int}) and GB

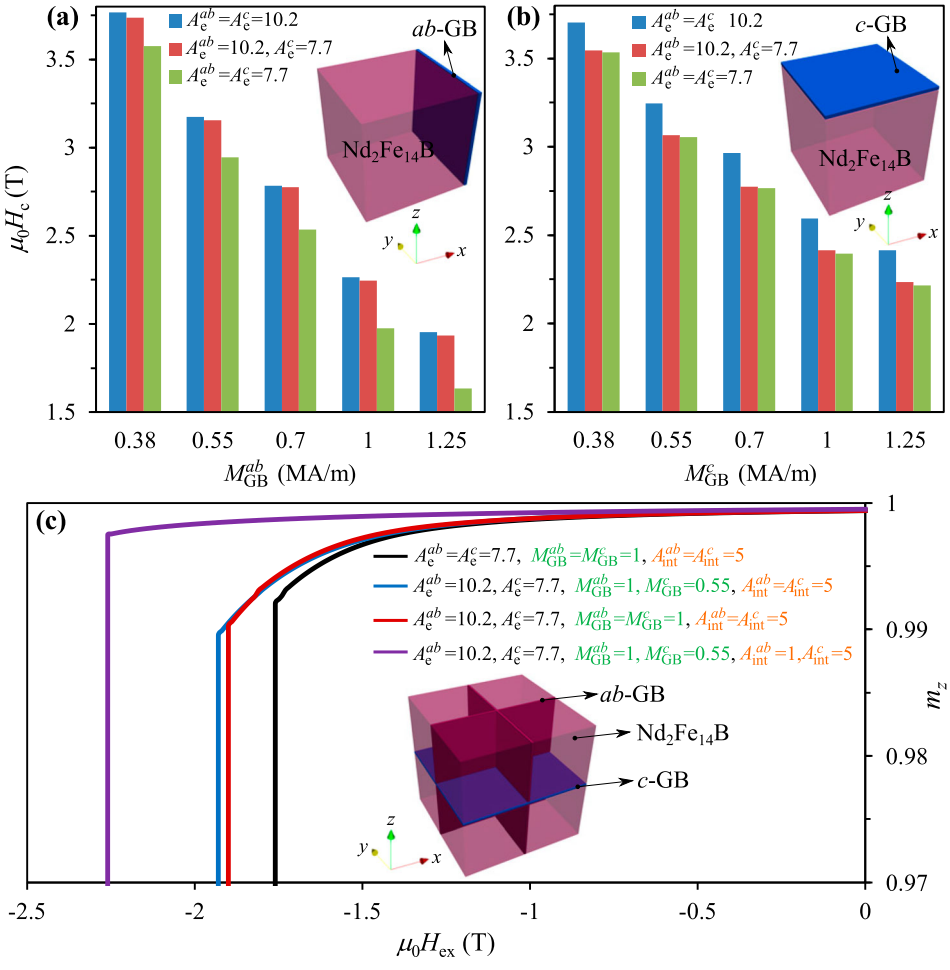

Figure 4. Dependency of coercivity on anisotropic exchange. Effect of anisotropic exchange stiffness of $Nd_2Fe_{14}B$ (A_e) in single grain with GB at (a) a surface and (b) c surface (with the same $A_{\text{int}} = 5$ pJ/m). (c) Effect of A_e, GB composition anisotropy, and anisotropic exchange coupling between two regions (A_{int}) in multigrain Nd–Fe–B. A_e and A_{int}: pJ/m. M_{GB}: MA/m. Grain size: 100 nm. GB thickness: 4 nm. The external field is applied along negative z axis.

composition on the coercivity in an 8-grain microstructure is summarized in Figure 4(c). It can be found that A_e anisotropy alone increases $\mu_0 H_c$ by 0.17 T when compared to the case of isotropic $A_e = 7.7$ pJ/m. GB composition anisotropy alone slightly improves $\mu_0 H_c$ by 0.03 T. When both the anisotropy in A_e and GB composition have been taken into account, the additional consideration of interface exchange anisotropy can remarkably enhance $\mu_0 H_c$ by 0.33 T. These results imply that the aforementioned exchange anisotropy has profound influence on the coercivity. It is thus necessary for the community of micromagnetic simulations to include these anisotropies in order to realize a reasonable design or prediction.

4. Conclusion

In conclusion, we have identified the exchange anisotropy and its influence on the coercivity of Nd–Fe–B magnets by using multiscale simulations. The exchange stiffness in $Nd_2Fe_{14}B$ phase is found to be intrinsically anisotropic (i.e. depend on the crystallographic axis) and its value along *c* axis is lower than along *a*/*b* axis. We discover the 'double anisotropy' phenomenon regarding to GB, i.e. in addition to the experimentally determined anisotropy in GB composition or magnetization, the interface exchange coupling strength between $Nd_2Fe_{14}B$ and GB is also confirmed to be strongly anisotropic. Due to this 'double anisotropy', the ferromagnetic exchange coupling for (001) interface is much weaker than that for (100) interface. The coercivity of Nd–Fe–B magnets is demonstrated to be obviously influenced by the exchange anisotropy, suggesting the necessity of including exchange anisotropy in order to realize a reasonable design or prediction by micromagnetic simulations. Overall, these findings in our Letter not only provide comprehensive understanding of exchange in Nd–Fe–B magnets but also are useful in deciphering coercivity mechanism and inspiring a strategy of tailoring exchange for the design of high-performance Nd–Fe–B permanent magnets.

Disclosure statement

No potential conflict of interest was reported by the authors.

Funding

This work was supported by the (Deutsche Forschungsgemeinschaft) German Science Foundation [grant numbers DFG YI 165/1-1, DFG XU 121/7-1, DFG SFB/TRR 270], the German federal state of Hessen through its excellence programme LOEWE "RESPONSE", the Lichtenberg High Performance Computer of TU Darmstadt, the 15th Thousand Youth Talents Program of China, the NSFC [grant number 11902150], the Research Fund of State Key Laboratory of Mechanics and Control of Mechanical Structures [grant number MCMS-I-0419G01], and a project Funded by the Priority Academic Program Development of Jiangsu Higher Education Institutions.

ORCID

Min Yi http://orcid.org/0000-0001-7672-3107
Oliver Gutfleisch http://orcid.org/0000-0001-8021-3839

References

[1] Gutfleisch O, Willard MA, Brück E, et al. Magnetic materials and devices for the 21st century: stronger, lighter, and more energy efficient. Adv Mater. 2011;23(7):821–842.
[2] Peng RC, Hu JM, Yang T, et al. Switching the chirality of a magnetic vortex deterministically with an electric field. Mater Res Lett. 2018;6(12):669–675.
[3] Bennett S, Herklotz A, Cress C, et al. Magnetic order multilayering in FeRh thin films by He-Ion irradiation. Mater Res Lett. 2017;6(1):106–112.
[4] Rivin O, Caspi E, Pesach A, et al. Evidence for ferromagnetic ordering in the MAX phase $(Cr_0.96Mn_0.04)_2GeC$. Mater Res Lett. 2017;5(7):465–471.
[5] Hono K, Sepehri-Amin H. Prospect for HRE-free high coercivity Nd-Fe-B permanent magnets. Scr Mater. 2018;151:6–13.
[6] Skokov K, Gutfleisch O. Heavy rare earth free, free rare earth and rare earth free magnets-vision and reality. Scr Mater. 2018;154:289–294.
[7] Hirosawa S, Nishino M, Miyashita S. Perspectives for high-performance permanent magnets: applications, coercivity, and new materials. Adv Nat Sci Nanosci Nanotechnol. 2017;8(1):013002.
[8] Yi M, Zhang H, Gutfleisch O, et al. Multiscale examination of strain effects in Nd-Fe-B permanent magnets. Phys Rev Appl. 2017;8(1):014011.
[9] Hrkac G, Woodcock TG, Freeman C, et al. The role of local anisotropy profiles at grain boundaries on the coercivity of $Nd_2Fe_{14}B$ magnets. Appl Phys Lett. 2010;97(23):232511.
[10] Bance S, Fischbacher J, Schrefl T, et al. Micromagnetics of shape anisotropy based permanent magnets. J Magn Magn Mater. 2014;363:121–124.
[11] Erokhin S, Berkov D. Optimization of nanocomposite materials for permanent magnets: micromagnetic simulations of the effects of intergrain exchange and the shapes of hard grains. Phys Rev Appl. 2017;7(1):014011.
[12] Yi M, Gutfleisch O, Xu BX. Micromagnetic simulations on the grain shape effect in Nd-Fe-B magnets. J Appl Phys. 2016;120(3):033903.
[13] Sepehri-Amin H, Ohkubo T, Gruber M, et al. Micromagnetic simulations on the grain size dependence of coercivity in anisotropic Nd-Fe-B sintered magnets. Scr Mater. 2014;89:29–32.
[14] Liu J, Sepehri-Amin H, Ohkubo T, et al. Grain size dependence of coercivity of hot-deformed Nd-Fe-B anisotropic magnets. Acta Mater. 2015;82:336–343.

[15] Ohkubo T, Abe T, Hirosawa S, et al. Faceted shell structure in grain boundary diffusion-processed sintered Nd-Fe-B magnets. J Alloy Compd. 2014;617:884–892.
[16] Li W, Sepehri-Amin H, Ohkubo T, et al. Distribution of Dy in high-coercivity (Nd,Dy)-Fe-B sintered magnet. Acta Mater. 2011;59(8):3061–3069.
[17] Helbig T, Loewe K, Sawatzki S, et al. Experimental and computational analysis of magnetization reversal in (Nd, Dy)-Fe-B core shell sintered magnets. Acta Mater. 2017;127:498–504.
[18] Wu D, Yue M, Liu W, et al. Magnetic domain switching in Nd–Fe–B sintered magnets with superior magnetic properties. Mater Res Lett. 2018;6(4):255–260.
[19] Woodcock T, Ramasse Q, Hrkac G, et al. Atomic-scale features of phase boundaries in hot deformed Nd-Fe-Co-B-Ga magnets infiltrated with a Nd–Cu eutectic liquid. Acta Mater. 2014;77:111–124.
[20] Sawatzki S, Kübel C, Ener S, et al. Grain boundary diffusion in nanocrystalline Nd-Fe-B permanent magnets with low-melting eutectics. Acta Mater. 2016;115:354–363.
[21] Soderžnik M, Sepehri-Amin H, Sasaki T, et al. Magnetization reversal of exchange-coupled and exchange-decoupled Nd-Fe-B magnets observed by magneto-optical Kerr effect microscopy. Acta Mater. 2017;135:68–76.
[22] Skomski R, Coey J. Giant energy product in nanostructured two-phase magnets. Phys Rev B. 1993;48(21):15812.
[23] Hadjipanayis G, Withanawasam L, Krause R. Nanocomposite $R_2Fe_{14}B/\alpha$-Fe permanent magnets. IEEE Trans Magn. 1995;31(6):3596–3601.
[24] Skomski R. Nanomagnetics. J Phys Condens Matter. 2003;15(20):R841.
[25] Hirosawa S, Matsuura Y, Yamamoto H, et al. Magnetization and magnetic anisotropy of $R_2Fe_{14}B$ measured on single crystals. J Appl Phys. 1986;59(3):873–879.
[26] Durst KD, Kronmüller H. Determination of intrinsic magnetic material parameters of $Nd_2Fe_{14}B$ from magnetic measurements of sintered $Nd_{15}Fe_{77}B_8$ magnets. J Magn Magn Mater. 1986;59(1–2):86–94.
[27] Givord D, Li H. Magnetic properties of $Y_2Fe_{14}B$ and $Nd_2Fe_{14}B$ single crystals. Solid State Commun. 1993;88(11–12):907–910.
[28] Haskel D, Lang J, Islam Z, et al. Atomic origin of magnetocrystalline anisotropy in $Nd_2Fe_{14}B$. Phys Rev Lett. 2005;95(21):217207.
[29] Ogawa D, Koike K, Kato H, et al. Evaluation of interlayer exchange coupling in α-Fe(100)/$Nd_2Fe_{14}B$(001) films. J Korean Phys Soc. 2013;63(3):489–492.
[30] Toga Y, Moriya H, Tsuchiura H, et al. First principles study on interfacial electronic structures in exchange-spring magnets. J Phys Conf Ser. 2011;266(1):012046.
[31] Ogawa D, Koike K, Mizukami S, et al. Negative exchange coupling in $Nd_2Fe_{14}B$(100)/α-Fe interface. Appl Phys Lett. 2015;107(10):102406.
[32] Umetsu N, Sakuma A, Toga Y. First-principles study of interface magnetic structure in $Nd_2Fe_{14}B$/(Fe, Co) exchange spring magnets. Phys Rev B. 2016;93(1):014408.
[33] Sepehri-Amin H, Ohkubo T, Nagashima S, et al. High-coercivity ultrafine-grained anisotropic Nd–Fe–B magnets processed by hot deformation and the Nd–Cu grain boundary diffusion process. Acta Mater. 2013;61(17):6622–6634.
[34] Zickler GA, Fidler J, Bernardi J, et al. A combined TEM/STEM and micromagnetic study of the anisotropic nature of grain boundaries and coercivity in Nd-Fe-B magnets. Adv Mater Sci Eng. 2017;2017:6412042.
[35] Zickler GA, Fidler J. Nanocompositional electron microscopic analysis and role of grain boundary phase of isotropically oriented Nd-Fe-B magnets. Adv Mater Sci Eng. 2017;2017:1461835.
[36] Evans RF, Fan WJ, Chureemart P, et al. Atomistic spin model simulations of magnetic nanomaterials. J Phys Condens Matter. 2014;26(10):103202.
[37] Toga Y, Matsumoto M, Miyashita S, et al. Monte Carlo analysis for finite-temperature magnetism of $Nd_2Fe_{14}B$ permanent magnet. Phys Rev B. 2016;94(17):174433.
[38] Nishino M, Toga Y, Miyashita S, et al. Atomistic-model study of temperature-dependent domain walls in the neodymium permanent magnet $Nd_2Fe_{14}B$. Phys Rev B. 2017;95(9):094429.
[39] Toga Y, Nishino M, Miyashita S, et al. Anisotropy of exchange stiffness based on atomic-scale magnetic properties in the rare-earth permanent magnet $Nd_2Fe_{14}B$. Phys Rev B. 2018;98(5):054418.
[40] Gong Q, Yi M, Evans R, et al. Calculating temperature-dependent properties of $Nd_2Fe_{14}B$ permanent magnets by atomistic spin model simulations. Phys Rev B. 2019;99(21):214409.
[41] Gong Q, Yi M, Xu BX. Multiscale simulations toward calculating coercivity of Nd-Fe-B permanent magnets at high temperatures. Phys Rev Mater. 2019;3(8):084406.
[42] Tatetsu Y, Tsuneyuki S, Gohda Y. First-principles study of the role of Cu in improving the coercivity of Nd-Fe-B permanent magnets. Phys Rev Appl. 2016;6(6):064029.
[43] Toga Y, Suzuki T, Sakuma A. Effects of trace elements on the crystal field parameters of Nd ions at the surface of $Nd_2Fe_{14}B$ grains. J Appl Phys. 2015;117(22):223905.
[44] Suzuki T, Toga Y, Sakuma A. Effects of deformation on the crystal field parameter of the Nd ions in $Nd_2Fe_{14}B$. J Appl Phys. 2014;115(17):17A703.
[45] Vansteenkiste A, Leliaert J, Dvornik M, et al. The design and verification of MuMax3. AIP Adv. 2014;4(10):107133.
[46] Kronmüller H, Fähnle M. Micromagnetism and the microstructure of ferromagnetic solids. Cambridge University Press, Cambridge, 2009.
[47] Ono K, Inami N, Saito K, et al. Observation of spin-wave dispersion in Nd-Fe-B magnets using neutron brillouin scattering. J Appl Phys. 2014;115(17):17A714.
[48] Sakuma A, Suzuki T, Furuuchi T, et al. Magnetism of Nd-Fe films as a model of grain boundary phase in Nd-Fe-B permanent magnets. Appl Phys Express. 2015;9(1):013002.
[49] Murakami Y, Tanigaki T, Sasaki T, et al. Magnetism of ultrathin intergranular boundary regions in Nd-Fe-B permanent magnets. Acta Mater. 2014;71:370–379.
[50] Sepehri-Amin H, Ohkubo T, Shima T, et al. Grain boundary and interface chemistry of an Nd-Fe-B-based sintered magnet. Acta Mater. 2012;60(3):819–830.